A structural study of gallium lanthanum sulphide glass bulk and thin films by x-ray absorption fine structure spectroscopy

1997 J. Phys.: Condens. Matter 9 6217

(http://iopscience.iop.org/0953-8984/9/29/007)

J. Phys.: Condens. Matter **9** (1997) 6217–6230. Printed in the UK PII: S0953-8984(97)82842-1

A structural study of gallium lanthanum sulphide glass bulk and thin films by x-ray absorption fine structure spectroscopy

R Asal†, P E Rivers and H N Rutt

Infrared Science and Technology, Department of Electronics and Computer Science, University of Southampton, Highfield, Southampton SO17 1BJ, UK

Received 24 March 1997

Abstract. Atomic-scale structure changes in gallium lanthanum sulphide bulk glass and ablation-deposited thin films have been studied by the x-ray absorption fine-structure (EXAFS) technique. EXAFS spectra have been recorded at the sulphur and gallium K edges, and the lanthanum L_3 edge, and this has allowed us to construct a detailed picture of the local structure in bulk glass and thin films. The EXAFS results indicate that there is chemical disorder in the structural network of the GLS thin films, although chemical ordering is predominant in bulk GLS glass. The existence of 'wrong bonds', i.e. Ga–Ga and S–S bonds, in the structure has been discussed and correlated with optical absorption experiments undertaken on the same samples to provide a consistent picture of the local structure.

1. Introduction

Glasses based on gallium lanthanum sulphide (GLS) have received increasing attention due to their wide range of novel opto-electronic applications [1–5]. The glasses are stable, hard, and non-hygroscopic, and the high lanthanum content is readily partially substituted for with other lanthanide dopants. When doped with rare earths such as Nd^{3+} and Er^{3+}, these glasses, by virtue of their low phonon energy and high refractive index (2.4), open up the possibility of operating lasers in the mid-infrared, and the use of energy levels which are non-radiatively quenched in oxide glasses. In addition, the GLS glasses exhibit a wide range of interesting photostimulated properties. These include subtle effects such as shifts in the absorption edge, and more substantial atomic and molecular reconfigurations such as photoinduced refractive index changes [6, 7]. The permanent changes in refractive index induced by illumination can be up to 1%. This leads to the possibility of writing high-spatial-resolution grating structures and waveguides.

Although the GLS glasses have potentially important applications as mentioned above, little is known about their structures. Benazeth *et al* [8] previously studied the structure of the bulk glasses using EXAFS at the gallium K edge and lanthanum L_3 edge (no sulphur edge measurements were reported). Their results show that the gallium atoms in the glass exist as tetrahedral networks of GaS_4, and that the Ga–S distances in the glasses are identical to those in the crystalline form of Ga_2S_3. The lanthanum environment is also very similar to that present in the crystalline state of $La_6Ga_2Mn_2S_{14}$. On the basis of the above findings,

† E-mail: raa@ecs.soton.ac.uk.

0953-8984/97/296217+14$19.50

Benazeth *et al* [8] suggested a possible structural model for these glasses. The gallium and sulphur environment in crystalline Ga_2S_3 is such that two of the three sulphur atoms are linked to three gallium atoms and the third sulphur atom is linked to two gallium atoms. The bonds that link two of the three sulphur atoms to three gallium atoms consist of two covalent bonds and a third dative bond, while the third sulphur atom linked to two gallium atoms represents the bridging atom. The addition of La_2S_3 brings in an additional S^{2-} anion that results in modification of the dative bond of the trigonally coordinated sulphur atom. The dative bond is broken, and then the S^{2-} anion brought in by the modifying rare-earth sulphide helps in restoring and maintaining the tetrahedral environment of GaS_4, at the same time creating a negative site for the La^{3+} cation. A schematic representation of the structures described by Benazeth *et al* can be found in reference [8].

Lucazeau *et al* [9] also studied the structure of these glasses using Raman spectroscopy. The Raman spectra of the glasses and of similar crystalline phases were compared, and spectral differences were noted between the two glassy and crystalline states. This has been interpreted in terms of structural modification of the short-range periodicity around the Ga atoms, although there is no conclusive evidence for this.

Despite their attractive properties, GLS glasses are of limited interest as materials for bulk glass lasers, because of the poor thermal properties of the glass, and interest centres on fibre-optic and planar waveguide devices. Such devices offer a possible means of incorporating sources and amplifiers into integrated optical circuits. The interest in these devices lies in exploiting the advantages offered by the planar geometry and the optical properties of rare-earth ions. For example, wavelength-division multiplexers, distributed Bragg mirror or distributed feedback structures may be monolithically integrated to allow pumping and tuning of the lasers, complex multiple-cavity devices may be readily printed photolithographically, and gain regions may be selectively defined in the substrate.

In this study, the structure and local bonding configurations in bulk GLS samples and ablation-deposited thin films have been investigated, for the first time, systematically as a function of deposition energy density (fluence) at the target, by means of EXAFS measurements. The data are unusual in that they include EXAFS data derived from all three elements present, allowing a detailed picture of the glass structure to be derived, and internal consistency checks. Our results show that gallium is always fourfold coordinated in the GLS network. Both Ga–Ga and S–S bonds occur in GLS thin-film samples, but the lanthanum atoms remain coordinated by sulphur alone. The EXAFS results, for bulk GLS, are in good agreement (within experimental error) with that found by Benazeth *et al* [8]. A correlation between the EXAFS results and the optical data is established.

2. Experimental procedure

The gallium–lanthanum–sulphur (GLS) thin films were prepared by the laser ablation technique using a GLS glass rotating target of 2.5 cm diameter in a vacuum chamber at a base pressure of 10^{-7} mbar. The pressure remains below 10^{-6} mbar during deposition; the system uses oil-free pumping and substrate load locking to minimize film contamination. To minimize pump-down time, the chamber was at all times vented with oxygen-free nitrogen. The target composition was $70Ga_2S_3$–$30La_2S_3$ (molar ratio), and it was fabricated in our laboratory. The sulphide powders were specially prepared by Merck Ltd for this work, and the powders were weighed and mixed under dry nitrogen. The starting mixture was loaded into a vitreous carbon crucible pre-placed in a silica ampoule. The ampoule was pumped down to a vacuum of 10^{-7} mbar and sealed, then heated in a furnace at 1200 °C for four hours, and then water quenched. The resulting glass targets were released readily from the

crucible, and were transparent and homogeneous. All of the films used in this study were prepared from the same target.

As the adhesion of the ablated material is greatly influenced by the nature of the substrate surface, all of the substrates were handled carefully and cleaned prior to loading into the chamber. All of the substrates were washed in acetone and then ultrasonically cleaned in methanol. The substrates used were microscope glass for optical (visible/uv) measurements, CaF_2 for IR measurements, and aluminium foil for microprobe analysis. The substrates were oscillated over ± 2 cm to improve film uniformity. The compositions of the samples were determined by a DS 130 scanning electron microscope (SEM) to which an energy-dispersive x-ray analyser (EDAX) was attached. No significant variations in composition were found between different areas of the same samples, showing that the GLS films were compositionally homogeneous, at least down to a scale of 5 μm $\times$ 5 μm (the area probed by the EDAX measurements). Transmission electron microscope measurements yielded electron diffraction patterns consisting of only a few diffuse rings, indicating that the ablated GLS films were amorphous.

The thicknesses of the films were determined both by an optical technique, in which the interference fringes in reflection were used, and by a mechanical method using a Talysurf. The results agreed to within 3%.

The output of a KrF excimer laser of 248 nm wavelength operating at 5 Hz and 700 mJ was focused by a uv-grade planoconvex lens of 50 cm focal length, was brought into the chamber through a fused silica window, and was incident at an angle of 45° on the target. The beam energy density was varied by changing the laser spot size on the target by altering the lens-to-target distance, whilst keeping the laser operating conditions constant. The target-to-substrate distance was 8 cm. The deposition rate was in the range 12–24 nm min^{-1} (depending on the energy density at the target). All of the films were deposited at room temperature, as optical studies [10] have shown this to provide the widest optical gap and lowest Urbach tail as measured optically.

The EXAFS measurements on the GLS were carried out using the 2 GeV synchrotron radiation source at the CLRC Laboratory at Daresbury. The beam currents during data collection were between 150 and 250 mA.

The sulphur K-edge data were obtained on station 3.4 (SOXAFS), which has a chromium-plated mirror to focus the beam at the sample. The mirror also has a high-energy reflectivity cut-off at about 3.5 keV so harmonic contamination of the monochromatic beam is minimal. The energy of the x-ray beam was defined using an InSb(111) double-crystal monochromator with harmonic rejection set at 70%. The sample has to be placed in an evacuated chamber (10^{-6} mbar), since soft or low-energy x-rays are appreciably attenuated in air, and the electron drain current method was used to measure the absorption coefficient μ [11]. This method requires conducting samples; hence, the thin-film samples were deposited onto copper substrates for these experiments. Bulk glass samples are of high resistivity, and the drain current method proved impractical. Measurements were made using powdered glass (30%) diluted in graphite and pressed into pellets by the drain current technique, or with bulk samples by means of x-ray fluorescence.

Measurements on the gallium K and lanthanum L_3 edges were performed on beam line 7.1 using a Si(111) double-crystal monochromator and a harmonic rejection of 50%. These experiments were performed in transmission mode, with detection by ionization chambers containing an argon–helium gas mixture. In this case, films 1–2 μm thick were deposited on Mylar substrates, and stacked to obtain the necessary sample thickness. The Mylar substrate absorbed little over the relevant x-ray range. The small samples required ($\sim$1 cm^2) for sulphur edge measurements were taken from the ablation plume centre. The large samples

($\sim 5 \times 5$ cm^2) needed for gallium and lanthanum measurements were centred on the plume. A more complete description of stations 7.1 and 3.4 may be found elsewhere [12].

Typical data acquisition times for EXAFS experiments were around 30 minutes, and at least three runs were taken for each sample as a consistency check. The data were summed after manual removed of occasional obvious glitches.

3. Data analysis

The EXAFS data were analysed in the standard way using the suite of programs available at the Daresbury Laboratory, notably EXCALIB, EXBACK, and EXCURV92 [13]. The EXCALIB program was used for summation of multiple data sets, and calibration of their edges and absorption. Pre- and post-edge backgrounds were removed by fitting low-order (1–3) polynomials to the appropriate regions of the experimental spectra using the program EXBACK. The normalized EXAFS function, $\chi(E)$, was first converted into $\chi(k)$ using

$$\frac{h^2k^2}{2m} = [E - E_{\text{edge}}] + E_0 \tag{1}$$

where E is the incident photon energy, E_{edge} is the threshold energy of that particular absorption edge, and E_0 is the energy offset, being the difference between the energy of a $k = 0$ photoelectron and the lowest unoccupied energy level. $\chi(k)$ is then multiplied by k^3 in order to compensate for the diminishing amplitudes of the experimental spectrum at high k-values. In order to obtain structural information, the program EXCURV92 was used to make a comparison of the least-squares fitting of the k^3-weighted experimental spectrum to the theoretical spectrum which was calculated using the rapid-curved-wave theory [14, 15]. The basic formula describing the theoretical EXAFS spectra for K edges is [16]

$$\chi(k) = -\frac{A(k)}{k} \sum_j \frac{N_j}{{r_j}^2} |f_j(k,\pi)| \exp(-2\sigma_j^2 k^2) \exp\left(\frac{-2r_j}{\lambda}\right) \sin(2kr_j + 2\delta(k) + \psi_j(k)) \tag{2}$$

where k is the momentum of the photoelectron, and N_j is the number of atoms at a distance r_j each with a back-scattering amplitude $f_j(k,\pi)$. $A(k)$ is a correction factor for absorption events that do not result in EXAFS, such as multi-electron excitations. λ is the elastic mean free path of the photoelectron (only elastically scattered electrons can interfere). It is this factor which restricts the range of contributions to $\chi(k)$. The exponential term is a Debye–Waller factor in which σ_j^2 is the mean square variation in the interatomic distance between emitting and scattering atoms. This accounts for both thermal motion and static disorder. The term δ is the phase shift produced by the passage of the photoelectron through the emitting atom potential, and φ is the phase of the back-scattered wave.

Structural information was obtained by multi-parameter fitting of the experimental data to the EXAFS function in k-space. The parameters fitted were the bond length (r_j), the coordination number (N_j), the mean square variation in bond length (σ^2), and the position of the Fermi level (E_F). The amplitude reduction factor ($A(k)$), which takes into account events such as shake-up and shake-off processes at the central atom [16], is obtained from EXAFS data for a crystalline $Mn_6Ga_2Mn_2S_{14}$ sample taken at the same time as our glass samples. This factor was varied for the standard sample to obtain a most likely value for each atom type; its magnitude was fixed at this 'best' result thereafter. The useful energy range of the spectra extended to 500–600 eV for gallium and sulphur, and 400 eV for lanthanum above the edge, and Gaussian windows were used in the Fourier transformations. The result of a Fourier transformation is a series of peaks, one corresponding to each of the shells of

the atoms contributing to the EXAFS. There are also peaks due to noise in the spectrum, and to the effect of the finite data range (we shall discuss this point later).

Of critical importance in the analysis of EXAFS data is the decision as to the number of atomic shells that can be used. The deviation of the theoretical model from the experimental result can be quantified in terms of a fit index (FI) as shown in equation (3):

$$\mathrm{FI} = \frac{1}{N_p} \sum_{i=1}^{N_p} [(\chi_i(\mathrm{calc}) - \chi_i(\mathrm{exp}))k^n]^2 \tag{3}$$

where N_p is the number of data points in the spectrum, and n is a k-weighting factor, which was kept at 3 throughout this work. Addition of an extra shell in the fitting procedure will decrease FI simply because of the increase in the number of variable parameters. We have therefore applied rigorous statistical tests in order to estimate the benefit of adding extra shells to the model. The same approach is applied in the evaluation of experimental errors. For a full discussion of these techniques the reader is referred to the paper by Joyner *et al* [17].

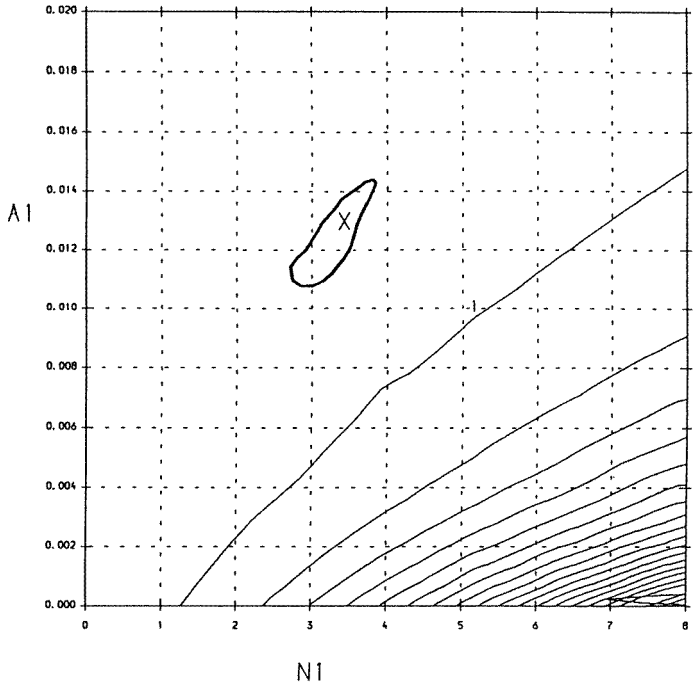

Figure 1. EXAFS error estimates for the first shell of a GLS thin-film sample (prepared at 3 J cm^{-2} energy density) based on Ga K-edge data. The contours show the fit index for the partial coordination number N1 and the Debye–Waller factor σ^2 (A1 $= 2\sigma^2$). The heavy contour encloses the 95% significance region as defined in the text.

The finite data range of our spectra leads to a correlation between some of the structural and other parameters. Examples are E_F and the interatomic distances, which define the phase of the EXAFS function, and the coordination number and Debye–Waller factor, which fix its amplitude. The presence of this correlation increases the uncertainty in our fit parameters. We have used the statistical method of Joyner *et al* [17] to obtain estimates of this uncertainty; the quality of the fit is determined in terms of the fit index, which is related

to the fit index minimum FI_{min} by $FI_{min}/FI < 0.96$. When we plot the fit index as a function of the values of two correlated variables we obtain a contour map with the minimum fit index defining the best-fit values. An example is shown in figure 1. The method Joyner *et al* allows us to determine the size of the region around this minimum where the fit is not significantly worse; roughly speaking, this corresponds to a change in the fit index of less than 5% for most of our EXAFS analyses.

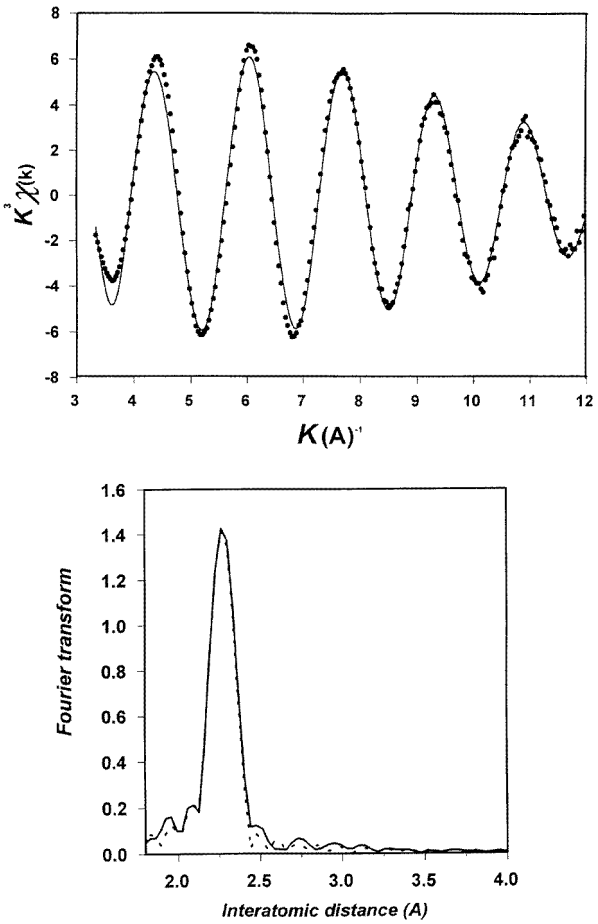

Figure 2. A typical example of a k^3-weighted EXAFS curve for the GLS thin-film sample (prepared at 3 J cm^{-2} energy density) at the Ga K edge, together with the corresponding Fourier transform. The dotted curves are the experimental results, and the solid curves represent the best fits to the data.

4. Results and discussion

4.1. Film structure

Figures 2, 3, and 4 give examples of the background-subtracted EXAFS functions $\chi(k)$, weighted by k^3, and their associated Fourier transforms. As always with EXCURV92 output, the Fourier transforms are phase corrected so that the peaks appear at the true interatomic

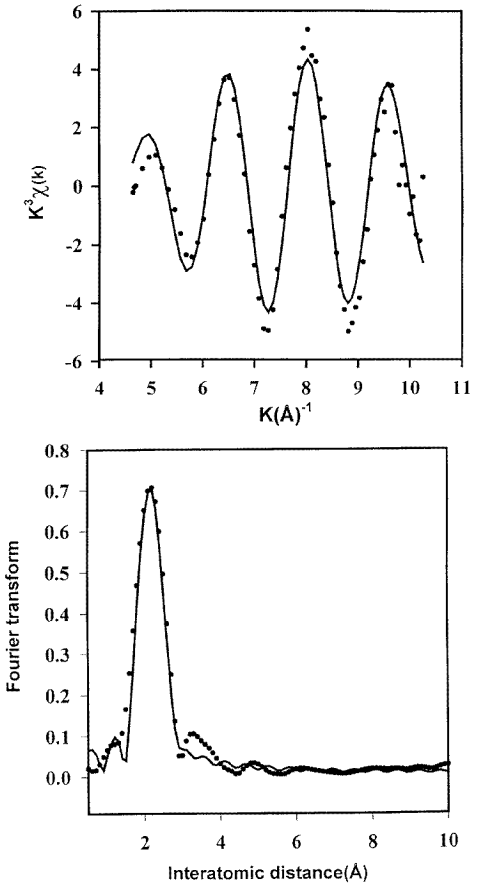

Figure 3. A typical example of a k^3-weighted EXAFS curve for the GLS thin-film sample (prepared at 3 J cm^{-2} energy density) at the S K edge, together with the corresponding Fourier transform. The dotted curves are the experimental results, and the solid curves represent the best fits to the data.

distances. In most of the cases described here, the noise level was sufficiently low to allow data out to $k = 10$–12 Å^{-1} to be used. The gallium K-edge spectra (figure 2) are typically excellent, with very good fitting to the observed spectra. The sulphur K-edge data (figure 3) are also generally good, but slightly inferior to the gallium edge data as regards signal-to-noise ratio and quality of fit. Typical lanthanum L_3-edge data are shown in figure 4. The relatively short data range for the La L_3-edge spectra was unavoidable, as the La L_2 edge lies only about 400 eV above the L_3 edge. The EXAFS spectra obtained from the La L_3-edge measurements each show an additional peak between 5 and 7 Å^{-1} due to double excitations involving the 2p and 4d electrons [18]. However, in spite of this we have still been able to analyse the La L_3-edge data. The La edge EXAFS spectra (a typical example is shown) have a remarkably constant phase and a slowly decreasing amplitude with increasing energy density, suggesting that the La environment is constant over this range.

Figures 5(a) and 5(b) show the gallium and sulphur, and lanthanum partial coordinations, and the total coordination numbers for gallium, $N_{\mathrm{Ga-T}}$, and sulphur, $N_{\mathrm{S-T}}$, as functions of the

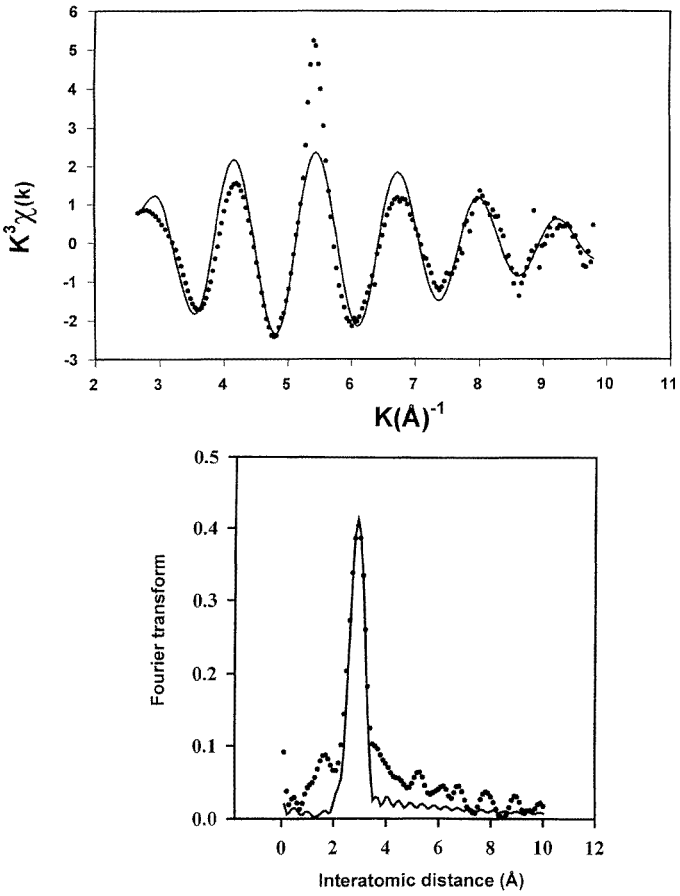

Figure 4. A typical example of a k^3-weighted EXAFS curve for the GLS thin-film sample (prepared at 3 J cm^{-2} energy density) at the La L_3 edge, together with the corresponding Fourier transform. The dotted curves are the experimental results, and the solid curves represent the best fits to the data.

energy density. The dotted horizontal lines in this figure and subsequent figures correspond to the values for the bulk glass sample. It can be seen that for the ablated films the partial coordination numbers of Ga, $N_{\mathrm{Ga-S}}$, and S, $N_{\mathrm{S-Ga}}$, decrease with increasing energy density. This behaviour may be interpreted as the breakage of Ga–S bonds and the formation of homopolar bonds ('wrong bonds'), i.e. Ga–Ga and S–S. This view is clearly supported by the associated increase in the Ga–Ga, $N_{\mathrm{Ga-Ga}}$, and S–S, $N_{\mathrm{S-S}}$, coordination numbers. It should be noted that, within the error limits indicated, the total gallium coordination $N_{\mathrm{Ga-T}}$ (obtained by summing the partial Ga coordinations) is approximately 4.0 throughout the energy density range studied. The fourfold total coordination of gallium in GLS samples, together with twofold sulphur, implies that the bonding is covalent, obeying Mott's 8N coordination rule [19]. By means of EXAFS measurements on GaAs flash-evaporated samples, Theye *et al* [20] and Del Cueto and Shevchik [21] did detect Ga–Ga bonds at distances of 2.46 ± 0.03 Å [20] and 2.45 Å [21]. The presence of 'wrong bonds' in evaporated As_2S_3 glass was also reported by Nemanich *et al* [22], and was interpreted by assuming that the As_4S_4 group was incorporated in the structure. Indeed, in the case of thin

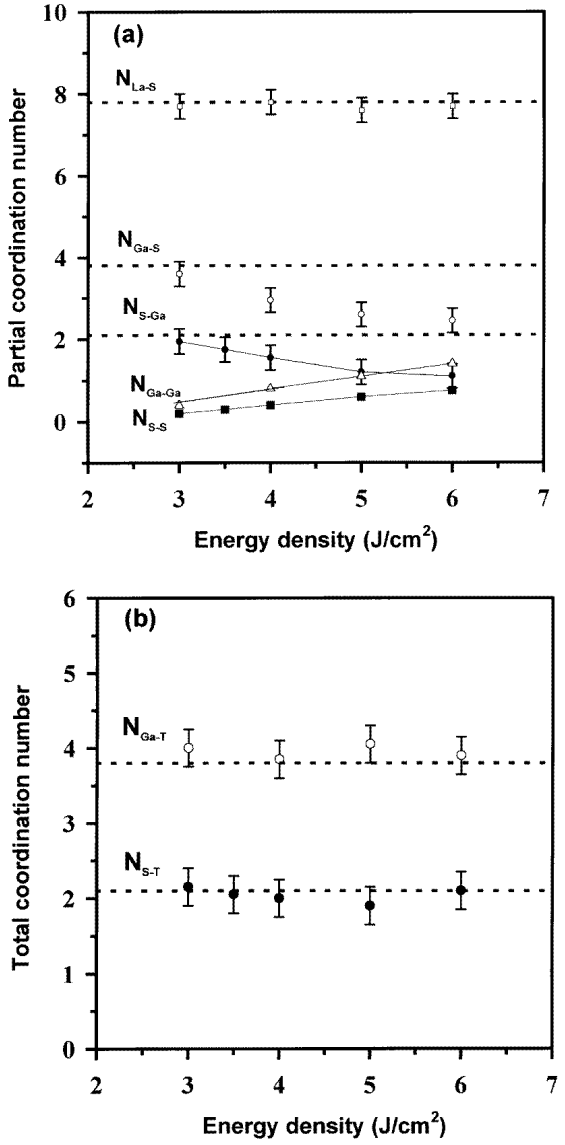

Figure 5. (a) The partial coordination numbers obtained from EXAFS data as functions of the energy density in GLS thin-film samples. (b) Total Ga and S coordinations as functions of the energy density. The solid lines are drawn as a guide to the eye.

films, 'wrong bonds' are almost impossible to avoid, and are undoubtedly linked to defect states within the band gap.

It is also clear from figure 5(a) that lanthanum (N_{La-S}) was always approximately eight-coordinated by sulphur, indicating that there is no observable change in the local environment of the La atoms. The EXAFS experiments could not detect any La–La bonds in any of our samples. Attempts to fit La–La bonds at 3.1 Å (the first-nearest-neighbour distance in metallic La) or at distances around 3.4 Å (twice the covalent radius of La) did not produce significant improvements to the fits. This could reflect a very large spread in

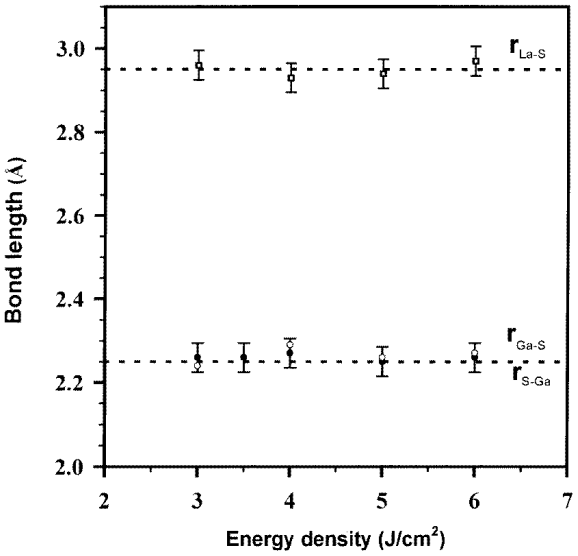

Figure 6. First-shell bond distances for GLS thin-film samples prepared at various ablation energy densities. Open circles denote Ga–S distances; solid circles denote S–Ga distances.

the bond length of any La–La bonds, or more probably a low level of La–La bonds.

The fitted values for the various bond lengths are plotted as a function of energy density in figure 6. $r_{\mathrm{Ga-S}}$ denotes the Ga–S interatomic distance fitted from Ga edge EXAFS data, while $r_{\mathrm{S-Ga}}$ represents the same bond length but deduced from S edge measurements; $r_{\mathrm{La-S}}$ is the La–S bond length measured from the La L_3 edge. Inspection of the figure reveals that there is clearly consistency, within experimental error, between the experimental values of $r_{\mathrm{Ga-S}}$ and of $r_{\mathrm{S-Ga}}$. All of the bond lengths determined by our analysis were found to be independent of deposition energy density, and, within their uncertainties, essentially the same as those found for the bulk glass. This shows that the mean bond length is unaffected by the type of the bonds surrounding each atom. The lengths of the Ga–Ga and S–S bonds, as determined from our EXAFS analysis, were found to be 2.8 ± 0.02 Å and 1.9 ± 0.02 Å respectively. The values reported for the Ga–Ga bond length are 2.76 Å in amorphous Ga [23] and 2.48 Å for dimers in crystalline orthorhombic Ga [24]. The close similarity of our measured bond lengths to those of stoichiometric materials strongly suggests that the covalent bonds are well defined and unchanging entities in thin-film samples.

The mean square deviation in nearest-neighbour distances (Debye–Waller factors), σ^2, are shown in figure 7. $\sigma^2_{\mathrm{Ga-S}}$ and $\sigma^2_{\mathrm{S-Ga}}$, the Debye–Waller factors for Ga–S bonds determined from Ga and S edge data, respectively, are clearly consistent with one another at all energy densities, within experimental error. This is expected, since they both show the spread of the same bond length, namely the Ga–S bond, and thus provide a consistency check on the fitted values. The values of $\sigma^2_{\mathrm{Ga-S}}$ and $\sigma^2_{\mathrm{S-Ga}}$ increase with increasing energy density, indicating an increase in the configurational (static) disorder of the bond length. This result is also consistent with optical data, where the Urbach parameter (disorder parameter) is seen to increase with increasing deposition energy density [10]. For amorphous structure, the Debye–Waller factor determined experimentally has contributions from both thermal and static disorder: $\sigma^2_{(\mathrm{exp})} = \sigma^2_{\mathrm{thermal(cryst)}} + \sigma^2_{\mathrm{static}}$. In the crystalline state, the above equation becomes $\sigma^2_{(\mathrm{exp})} = \sigma^2_{\mathrm{thermal(cryst)}}$ which allows us to estimate the static disorder of

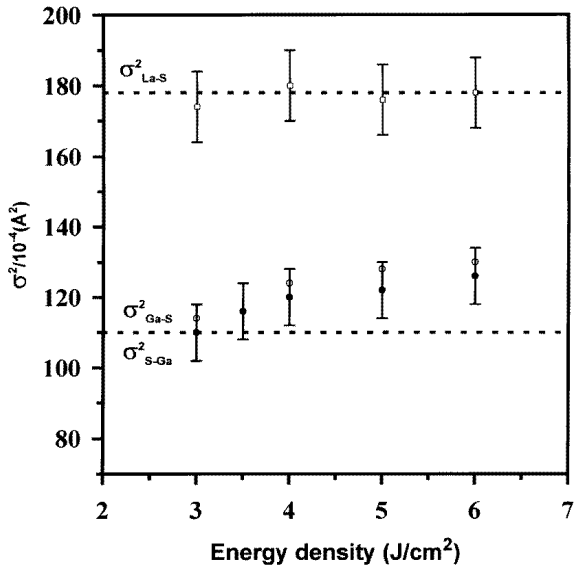

Figure 7. The energy density dependence of the mean square deviation in interatomic distances, σ^2, obtained from the EXAFS data for GLS samples. Open circles denote σ^2_{Ga-S}, and solid circles denote σ^2_{S-Ga}.

the amorphous materials. From our EXAFS analysis on the standard (crystalline) sample, the Debye–Waller factor for Ga–S was found to be 54×10^{-4} Å^2. By comparing this value with observed sample values (figure 7), we can conclude that there is a considerable static disorder in the Ga–S bond length in our samples. It is also clear from the data presented in figure 7 that there is no significant change in Debye–Waller factor for La–S bonds, σ^2_{La-S}, with energy density, and that, within experimental error, they are the same as that found in bulk glass. This suggests that the configurational disorder in the local environment of the La atoms remains much the same across the energy density range studied. The room temperature thermal contribution to σ^2 for the La–S bond is equal to 150×10^{-4} Å^2 (the value for the crystalline sample). Therefore, there is very little static disorder in the La–S bond length in our samples. The Debye–Waller factors for Ga–Ga and S–S bonds in our thin-film samples remain low (90×10^{-4} Å^2 and 70×10^{-4} Å^2 respectively) at all deposition energy densities, indicating that bond-length disorder for these bond types is low. To our knowledge, there are no data available in the literature for comparison.

Our EXAFS data reveal a degree of chemical disorder in the structural network of the ablation-deposited GLS films. Two basic models can be used to describe the glass structure. The first is the random-bond network (RBN) model [25]. In this model, the distribution of bonds is purely statistical, and is completely determined by the composition. The second model is the ordered-bond network (OBN) model, which assumes that bonds between unlike atoms are favoured, and complete chemical ordering occurs at the stoichiometric compositions [26]. As we have seen in figure 5(a), the number of the 'wrong bonds' slowly increases with increasing energy density. There is clear evidence that this reflects a gradual change from the predominantly tetrahedral OBN structure at low energy density (<4 J cm^{-2}) to the RBN network at high energy density (>4 J cm^{-2}). The presence of a high percentage of 'wrong bonds' in our thin-film samples provides strong evidence that

the system is chemically disordered, and that a non-stoichiometric network is obtained. The question of chemical order or disorder can also be examined by making use of the fact that the number of Ga–S bonds must be the same whether viewed from a gallium or sulphur atom. This leads to the condition

$$C_{\mathrm{Ga}} N_{\mathrm{Ga-S}} = C_{\mathrm{S}} N_{\mathrm{S-Ga}}$$

where C_{Ga} is the Ga content and C_{S} is the S content. This criterion has been applied to GLS thin-film samples by using the coordination numbers determined from the EXAFS, and the composition values obtained from the EDAX. It was found that the above equation is not satisfied. Therefore, again we conclude that GLS thin film is chemically disordered. The 'wrong bonds' are expected to give rise to states near the valence- and conduction-band edges, which inevitably results in a reduction in the band gap, and hence a shift of the absorption edge towards lower energies. Indeed, our optical measurements have shown that the optical gap decreases with increasing energy density, and the absorption edge becomes very broad and shifts to lower energy [10].

4.2. Film growth mechanisms

The EXAFS results clearly indicate that the deterioration in the properties of the films produced at high energy density is a result of Ga–Ga and S–S 'wrong bonds', whilst the La coordination remains identical to that of the bulk glass to within experimental error. Although at low energy density the level of 'wrong bonds' falls below the EXAFS detection limit, the overall trends strongly suggest that significant densities of these defects remain even in films prepared at low deposition energy density. It is also clear that this chalcogenide system is very much more difficult to ablate as a low-defect-density film than the extremely wide range of oxide-based materials which have been successfully ablated [27]. Discussion of ablated film growth mechanisms to date has centred on epitaxial growth, or growth of polycrystalline films, invariably for oxide species. We present here a preliminary interpretation of the mechanisms leading to difficulties in the growth of our glassy, chalcogenide films in terms of the electronegativity differences and 'bond energies' of the species present. This interpretation applies primarily to film growth from neutral atoms. Whilst these form a major constituent of the plume, the presence of molecular species at low energies and that of ions at high energies represent additional complications not addressed here.

In table 1 we collect together the heats of formation from the elements, and the electronegativity differences between the metal and sulphur for the two constituent sulphides comprising the glass and for the corresponding oxides [28–30]. The heat of formation 'per bond' is calculated assuming six nominal bonds per molecule, with a formal valency of three for the metal and two for the sulphur. The use of this metal–metal bond energy is clearly a rough approximation. Although no studies have been conducted of the ablation plume dynamics in GLS, the energy of the species arriving at the substrate is typically in the region one to four electron volts [31], with a tail component extending to high energies, increasing with the laser energy density [32]. The internal electronic excitations of the ablating species are also expected to be in the region of a few electron volts. This suggests that species arriving with energies significantly in excess of the bond energy are not readily captured, thus causing the lanthanum coordination to remain the same as that in the bulk, whilst the gallium coordination is partially changed. The electronegativity difference between the metal and sulphur or oxygen can also be used as an indication of the bond strength, yielding the same correlation. In further support of this hypothesis we note that most readily ablated

oxide species [27] have far higher energies per bond, and that, in the presence of low partial pressures of oxygen, GLS films grow much more quickly, and have a higher oxygen content, a wider optical gap, and less Urbach tail absorption [10]. The much faster growth rate in this case shows that the sticking coefficient for GLS growth in vacuum is much less than unity but increases under oxygen, again an indication of the importance of the bond energy as compared to the ablating species energy.

Table 1. Heats of formation, bond energies, and the electronegativity difference relevant to GLS film growth mechanisms.

Compound	Heat of formation (kJ mol^{-1})	Heat of formation (eV/molecule)	Heat of formation per bond (eV)	Electronegativity difference (eV) (Allred and Rochow [33])
La_2S_3	1222	27.6	4.6	−1.3
Ga_2S_3	516	22.8	3.8	−0.6
La_2O_3	1916	35.09	5.8	−2.4
Ga_2O_3	1079	29.8	3.7	−1.7
Ga–Ga	276	2.9	0.95	0
La–La	368	3.8	1.3	0
La–Ga	?	?	?	−0.7

Overall, these results suggest that chalcogenide systems will in general be more difficult to ablate as stoichiometric, chemically ordered films than as oxides. Conditions should be chosen so as to minimize the ablating species energy by using energy densities close to threshold, and where feasible the bond energies should be maximized. As a possible example of this, substitution of aluminium for gallium in GLS may improve the ablated film, but with the disadvantage of increased moisture sensitivity.

5. Summary

In this paper, the local structure and bonding environments of the Ga, S, and La atoms in bulk GLS glass and laser-ablation-deposited thin-film GLS have been investigated by means of EXAFS experiments; the absorption edges of all three components were measured. Values for the partial coordination number, bond lengths, and Debye–Waller factors determined from the different absorption edges were consistent with one another.

The EXAFS results for thin-film samples indicate that there is a significant change in the local environment of the Ga atom as the deposition energy density is increased, and the structure appears to be chemically disordered, with Ga–Ga bonds favoured due to their lower configuration energy. Optical data are consistent with this.

The bond lengths were found to be independent of the energy density, and were the same as those found for bulk glass. Although the nearest neighbour is well defined, there is a considerable bond-angle variation, and hence a wide variation in second-neighbour distance.

The Debye–Waller factors for Ga–S determined from both the Ga and S edges are consistent with each other, and vary appreciably with deposition energy density. There is a considerable static disorder in the Ga–S bond length, but little in the length of the La–S bond.

Acknowledgments

The authors are grateful to the CLRC for provision of synchrotron radiation and computing facilities at the Daresbury Laboratory. The bulk of the work was made possible by a grant from the EPSRC under grant reference GR/J40805. We also wish to thank Dr D W Hewak for useful discussions, Dr Loireau-Lozac'h for supplying the standard sample of crystalline $La_6Ga_2Mn_2S_{14}$, and Merck Ltd, of Poole, UK, for the supply of high-quality sulphide powders.

References

[1] Asal R, Rivers P E and Rutt H N 1996 *Materials Research Society Symp. Proc.* vol 397, ed R Singh, D Norton, L Laude, J Narayan and J Cheung (Pittsburgh, PA: MRS) pp 253–8
[2] Gill D S, Eason R W, Zaldo C, Rutt H N and Vainos N A 1995 *J. Non-Cryst. Solids* **191** 321
[3] Quimby R S, Gahagan K T, Aitken B G and Newhouse M A 1995 *Opt. Lett.* **20** 2021
[4] Hewak D W, Moore R C, Schweizer T, Wang J, Samoson B, Brocklesy W S, Pane D N and Tarbox E J 1996 *Electron Lett.* **32** 384
[5] Simons D R, Faber A J and Waal D E 1995 *J. Non-Cryst. Solids* **185** 283
[6] Elliot S R 1986 *J. Non-Cryst. Solids* **81** 71
[7] Owen A E, Firth A P and Ewen P J S 1985 *Phil. Mag.* B **52** 347
[8] Benazeth S, Tuilier M H, Loireau-Lozac'h A M, Dexpert H, Lagarde P and Flahaut J 1989 *J. Non-Cryst. Solids* **110** 89
[9] Lucazeau G, Barnier S and Loireau-Lozac'h 1977 *Mater. Res. Bull* **12** 437
[10] Asal R and Rutt H N 1997 *Opt. Mater.* at press
[11] Elan W T, Kirkland J P, Neiser R and Wolf P D 1988 *Phys. Rev.* B **38** 26
[12] Morrel C, Campbell J C, Diakun G P, Dobson B R, Greaves G N and Hasnain S S (undated) *EXAFS Users' Manual* Daresbury Laboratory, UK
[13] Binsted N, Campbell J W and Gurman S J 1991 *EXCURV92* Daresbury Laboratory, UK (EXAFS analysis programs)
[14] Binsted N, Gurman S J and Ross I 1984 *J. Phys. C: Solid State Phys.* **17** 143
[15] Binsted N, Gurman S J and Ross I 1986 *J. Phys. C: Solid State Phys.* **19** 1845
[16] Lee P A and Pendry J B 1975 *Phys. Rev.* B **11** 2795
[17] Joyner R W, Martin K J and Meehan P 1987 *J. Phys. C: Solid State Phys.* **20** 4005
[18] Benazeth S, Tuilier M H and Guittard M 1989 *Physica* B **158** 39
[19] Mott N F and Davis E A 1979 *Electronics Processes in Non-Crystalline Materials* (Oxford: Oxford University Press)
[20] Theye M L, Gheorghiu A and Launois H 1980 *J. Phys. C: Solid State Phys.* **13** 6569
[21] Del Cueto J A and Shevchik N J 1978 *J. Phys. C: Solid State Phys.* **11** L829
[22] Nemanich R J, Connell G A N, Hayes T M and Street R A 1978 *Phys. Rev.* B **18** 6900
[23] Ichikawa T 1973 *Phys. Status Solidi* **19** 347
[24] Sharma B D and Donohue J 1962 *Z. Kristallogr.* **177** 293
[25] Gurman S J 1990 *J. Non-Cryst. Solids* **125** 151
[26] Philipp H R 1972 *J. Non-Cryst. Solids* **8** 627
[27] Chrisey D B and Hubler G K 1994 *Pulsed Laser Deposition of Thin Films* (New York: Wiley)
[28] Kaye G W C and Laby T H 1986 *Tables of Physical and Chemical Constants* 15th edn (New York: Longman)
[29] *Handbook of Chemistry and Physics* 1976 ed R C Weast (Cleveland, OH: Chemical Rubber Company Press)
[30] Mills K C 1974 *Thermodynamic Data for Inorganic Sulphides, Selenides and Tellurides* (London: Butterworth)
[31] Dreyfus W, Kelly R and Walkup R E 1986 *Appl. Phys. Lett.* **49** 1478
[32] Bykovskii Yu A, Sil'nov S M, Sotnichenko E A and Shestakov B A 1987 *Sov. Phys.–JETP* **66** 285
[33] Allred A L and Rochow E G 1958 *J. Inorg. Nucl. Chem.* **5** 264